Cellulose (2021) 28:6073–6087
https://doi.org/10.1007/s10570-021-03905-8

ORIGINAL RESEARCH

Simple functionalization of cellulose beads with pre-propargylated chitosan for clickable scaffold substrates

Diego Gomez-Maldonado · Ilari Filpponen · Javier A. Hernandez-Díaz · Matthew N. Waters · Maria L. Auad · Leena-Sisko Johansson · Iris B. Vega-Erramuspe · Maria S. Peresin

Received: 4 January 2021 / Accepted: 1 May 2021 / Published online: 22 May 2021

Abstract Concerning the increased market for bio-based materials and environmentally safe practices, cellulose-based beads are one of the more attractive alternatives. Thus, this work focuses on the generation of functional cellulose-based beads with a relatively simple and direct method of blending a pre-modified chitosan bearing the targeted functional groups and cellulose, prior to the formation of the beads, as a mean to have functional groups in the formed structure. To this end, chitosan was chemically modified with propargyl bromide in homogenous reaction conditions and then combined with cellulose in sodium hydroxide/urea solution and coagulated in nitric acid to produce spherical shaped beads. The successful chemical modification of chitosan was assessed by elemental analysis, as well as by Fourier-transform infrared spectroscopy, Raman spectroscopy and X-ray photoelectron spectroscopy. The alkynyl moieties from the chitosan derivative, served as reactive functional groups for click-chemistry as demonstrated by the tagging of the commercial fluorophore Azide-Fluor 488 via CuI-catalysed alkyne-azide cycloaddition reaction, in aqueous

Supplementary Information The online version contains supplementary material available at https://doi.org/10.1007/s10570-021-03905-8.

D. Gomez-Maldonado · J. A. Hernandez-Díaz · I. B. Vega-Erramuspe (✉) · M. S. Peresin (✉)
Forest Products Development Center, School of Forestry and Wildlife Sciences, Auburn University, 520 Devall Drive, Auburn, AL 36849, USA
e-mail: ibv0002@auburn.edu

M. S. Peresin
e-mail: soledad.peresin@auburn.edu

I. Filpponen
Department of Chemical Engineering, Alabama Center for Paper and Bioresource Engineering (AC-PABE), Auburn University, Auburn, AL 36849, USA

M. N. Waters
Department of Crop, Soil and Environmental Sciences, Auburn University, Auburn, AL 36849, USA

M. L. Auad
Department of Chemical Engineering, Center for Polymers and Advanced Composites, Auburn University, Auburn, AL 36849, USA

L.-S. Johansson
Department of Bioprocesses and Biosystems, School of Chemical Engineering, Aalto University, 00076 Espoo, Finland

media. This work demonstrates the one-step processing of multiple polysaccharides for functional spherical beads as a template for bio-based scaffolds such as enzyme immobilization for stimuli-response applications and bioconjugations.

Keywords Functional cellulose bead · Chitosan propargylation · Click-chemistry · Bio-based scaffolds · Low-density materials

Introduction

In the last few decades, a growing market for low carbon footprint products derived from green processes has been the focus of research worldwide. Current efforts on efficient ways to utilize biomass have been made, focusing on the generation of more sustainable and environmentally friendly products that can replace the existing fossil fuel derived commodities (Rojas 2014). Thus, the formation of cellulose-based structures with higher structural hierarchy—such as beads—(O'Neill Jr and Emerald 1951; Trygg et al. 2013; Trivedi et al. 2018) open possibilities for a wide variety of applications, such as packed column reactors, protein and enzymes immobilization, solid-phase synthesis, drug loading and release, and water treatment with expected low-production costs (Gericke et al. 2013; Park et al. 2015; Voon et al. 2015; Zambrano et al. 2020).

The processing of cellulose to produce these beads is limited to their solubility, which can then determine the shape and properties—like density and porosity—of the final products. The more prominent technology used is the solubilization of cellulose into ionic liquids (Pinkert et al. 2010; Elsayed et al. 2020; Reyes et al. 2020) and urea/sodium hydroxide solutions (Cai and Zhang 2006; Luo and Zhang 2010) from which dissolved cellulose is then regenerated into the spherical shapes.

Nevertheless, the use of this beads in high-end products is somehow limited to the reactions possible with the available surface hydroxyl functional groups, restricting to reactions such as esterification and etherification (French 2017). Alternatively, second step modifications have been performed in the formed beads, most commonly TEMPO oxidation of the beads to have surface carboxyl groups to add charge and functionality (Blachechen et al. 2014; Trygg et al. 2014; de Carvalho et al. 2016; Fujii et al. 2020; Tan et al. 2020; Wu and Andrews 2020). However, this adds steps and energy inputs to the process, increasing the carbon footprint and cost, and limiting again the possible surface groups to moieties such as acetate, hydroxypropyl, methyl, carboxyl, xanthate and nitrate groups (Reis et al. 2019).

As an alternative, co-solutes can be added before the regeneration process as it has been explored with functional nanoparticles that can add properties such as magnetism (Luo et al. 2016), catalytic activity (Luo et al. 2016; Singh et al. 2019), or increase activity of other immobilized enzymes (Park et al. 2015). Still, to the best of our knowledge little exploration has been done with other polysaccharides as co-solutes (Wittmar et al. 2020) and even less with well characterized pre-modified polysaccharides with beneficial groups for green chemistry processes as a mean to add this moieties to the beads.

For this, the highly abundant chitosan (Kumar Dutta et al. 2004); and its amino functional group can be utilized and mixed with the cellulose to interact by either direct covalent coupling, by Van der Waals forces, or by electrostatic interactions with negatively charged counterparts (Struszczyk 2002; Kumar Dutta et al. 2004; Rinaudo 2006; Orelma et al. 2011).

As mentioned above, the amino-functional groups present in chitosan are susceptible to chemical modifications. Herein, we demonstrate that the amino functional groups of chitosan can react with propargyl bromide to introducing propargyl moieties in the polysaccharide chain, making the chitosan derivative suitable for click chemistry reaction. This click reaction selectively bind two moieties from different molecular building blocks in aqueous media, with no secondary reactions (Binder and Kluger 2006; Hoyle and Bowman 2010). To date, the most common click reaction utilized with carbohydrates is the copper(I) catalyzed azide-alkyne cycloaddition reaction CuAAC (Kolb et al. 2001; Liang and Astruc 2011). This reaction generates a stable triazole ring that serves both as a linker and as a spacer, under mild conditions. Consequently, thermolabile molecules such as proteins and ribonucleic acids can be linked without losing their specific structure, and therefore, their activity. This coupling reaction allows, for example, in vivo monitoring of the tagged molecules (Laughlin et al. 2008; Bart et al. 2009; Guan et al.

2011; Burnaevskiy et al. 2013). Moreover, the derivatization of chitosan with alkyne functional groups is a one-step reaction that offers multiple benefits (Kulbokaite et al. 2009; Ifuku et al. 2011, 2013; Guo et al. 2016).

The resulting beads then might be useful in multiple high-end fields such as catalysis, imaging, tissue engineering, drug delivery, soft robotics, or photo-responsive applications (Gonçalves et al. 2010; Ifuku et al. 2013; Hu et al. 2014).

In this work we used a propargylation reaction to introduce alkyne functional groups in the chitosan polymer chain (Guo et al. 2016). The synthetized chitosan derivative was blended with cellulose in alkaline conditions at − 10 °C, and the mixture was regenerated in acidic media to produce cellulose-based beads. The click-reaction was thereafter performed with the commercial fluorophore Azide-fluor 488 (A488), showing that these beads maintain the viability of the alkyne functional groups on the propargylated-chitosan intact. This is the first time that pre-modified chitosan is reported to be used in the formation of propargylated chitosan-cellulose spheres (pChS). Moreover, we have shown that alkynyl moieties can react with azido functional groups, demonstrating the potential of these spherical beads to be used as scaffold for clickable substrates.

The infographic of the work described in this paper is shown in Fig. 1. The chemical composition and thermal properties of chitosan and its derivative was evaluated using elemental analysis (EA), Fourier-transform infrared (FTIR) spectroscopy, Raman spectroscopy, X-ray photoelectron spectroscopy (XPS), and thermogravimetric analysis (TGA). The surface morphology of the beads was examined using scanning electron microscopy (SEM). And the success of the click reaction was corroborated by fluorescence microscopy and fluorescence spectroscopy.

Materials and methods

Materials

Dissolving pulp was kindly provided by a North American mill. Ethyl alcohol 190 proof and nitric acid ACS reagent grade were purchased from Pharmco-Aaper (Mississauga, Ontario, Canada). Hydrochloric acid (37% w/w) was obtained from Avantor-Macron (Radnor, Pennsylvania, US). Crystalized Urea was purchased from VWR (Radnor, Pennsylvania, US). Chitosan (85% deacetylated) and NaOH pearls (97% purity) were purchased from Alfa Aesar (Ward Hill, Massachusetts, US). Glacial acetic acid (99.9%) was purchased from Fisher Scientific (Pittsburgh, Pennsylvania, US). Propargyl bromide was purchased from TCI Chemicals (Tokyo, Japan). Azide-Fluor 488 was purchased from Aldrich (St. Louis, Missouri, US). Copper (II) sulfate pentahydrate (ACS grade) was purchased from BDH (Solon, Ohio, US), Ascorbic acid (reagent grade) was purchased from Sigma (St. Louis, Missouri, US). Hatman (Little Chalfont, Buckinghamshire, UK) Grade GF/A Glass Microfiber Filter particle retention in liquid 1.6 µm at 98% efficiency was also used for filtration in all steps. Spectra/Por®3 Dialysis membrane tubing with MWCO 3.5 KDa was purchased from Spectrum Chemical Mfg. (New Brunswick, New Jersey, US). Unless specified, all weight measurements in this paper are expressed on an oven-dry basis.

Pre-treatment of dissolving pulp

8 g of dissolving pulp were first rehydrated in ultrapure water at 4 °C overnight. The rehydrated pulp was stirred for 260 rpm for 1 h at ambient conditions, then filtered under vacuum, and mixed with 200 mL of 96% ethanol and 8 mL of HCl (37% w/w) at 75 °C for 2 h, under 200 rpm stirring. The resulting suspension was washed with ultrapure water until neutral pH. Subsequently, the filtrated slurry was placed in the dialysis membrane in a continuous dialysis system against ultrapure water, until the liquid in the reservoir achieved a conductivity value of 1.25 µS/cm or lower. The obtained pulp was once more filtrated and stored at 4 °C until further use.

Synthesis of the propargylated chitosan derivative

The propargylated chitosan was prepared modifying the protocol described by (Guo et al. 2016). Briefly, 12.7 g (107 mmol) of propargyl bromide was added dropwise to the chitosan suspension (10 mmol in 5% w/w NaOH solution) at 60 °C and stirred during 5 h. The reaction was stopped using 800 mL of ethanol/water solution (50/50 v/v). The chitosan derivative was filtered under vacuum and thoroughly washed with hot, fresh ethanol/water solution. The resulting

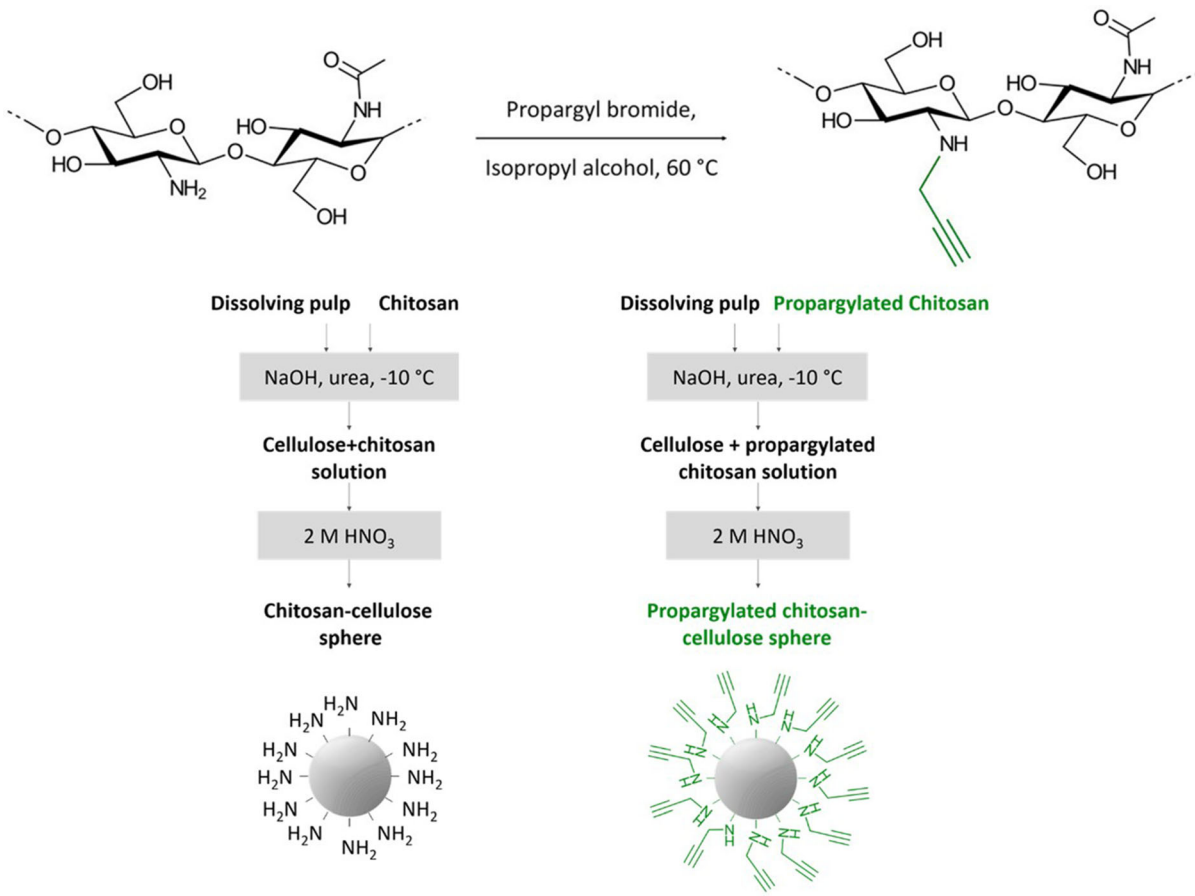

Fig. 1 Synthesis scheme for the preparation of propargylated chitosan polymer (top) and illustration of the paths followed for the fabrication of two different types of spherical beads

slurry was dried under vacuum at 50 °C and stored in a desiccator until further use.

Preparation of the spherical beads

Chitosan-cellulose spheres (ChS)

500 mg (2% w/v final cellulose content) of pretreated pulp (37% w/w solid content) was added to 25 mL of alkaline solution (7% w/w NaOH, 12% w/w urea, in water) at − 10 °C and 500 mg (2% w/v) of chitosan. Once dissolved, the cold solution was added dropwise to a 50 mL of 2 M nitric acid solution in a graduated cylinder. After 10 min in the coagulation bath, the obtained spheres were transferred into a reservoir with ultrapure water and thoroughly washed under a continuous flow of ultrapure water overnight.

Propargylated chitosan-cellulose spherical beads (p-ChS)

In 25 mL of alkaline solution (7% w/w NaOH, 12% w/w urea, in water) at − 10 °C, 500 mg of the propargylated chitosan and 500 mg of pretreated pulp were added to obtain a concentration of 2% w/v respectively. Once dissolved, the cold solution was added dropwise to 50 mL of 2 M nitric acid solution in graduated cylinders to allow coagulation. After 10 min, the spheres were transferred into a reservoir with ultrapure water and washed as described above.

Cu(I) catalyzed alkyne-azide click cycloaddition reaction

Propargylated-chitosan spheres (p-ChS) were subjected to Cu (I) catalyzed alkyne-azide click

cycloaddition reaction in aqueous media, under mild agitation at ambient conditions. For that purpose, 40 spheres were suspended in 10 mL of 5.0 mM A488 solution and mixed with 2.0 mL of 5.0 mM ascorbic acid and 2.0 mL of 1.0 mM of copper (II) sulfate. After two hours of reaction, these beads were thoroughly washed with water and stored at 4 °C in the dark until further use (referred to as p-ChS* in the "Discussion" section). A control sample ChS* was prepared following the same protocol, using chitosan spheres (ChS) instead of p-ChS beads.

Characterization techniques

Dry content

Chitosan-cellulose spheres were weighted in aluminum pans and placed in an oven at 105 °C overnight. The dry material was weighted, and percentage moisture content was calculated according to Eq. 1.

$$MC\% = \frac{mass_{wet} - mass_{dry}}{mass_{wet}} * 100\% \quad (1)$$

Tests were performed in triplicate, and the average value was calculated. Dry content was determined as the difference in the total mass (100%) and MC%. Size was obtained by measuring the diameter of the different spheres with a caliper, the values were then averaged.

Water retention and water uptake capacity measurements

The dried spheres were placed for 72 h in Petri dishes with 15 mL of ultrapure water, 15 mM NaCl, and phosphate saline buffer (PBS), at room temperature. After that, the spheres were weighed, and the percentage of water uptake was calculated according to Eq. 2.

$$Wateruptake\% = \frac{mass_{dry} - mass_{wet}}{mass_{dry}} * 100\% \quad (2)$$

Fourier-transform infrared spectroscopy (FTIR)

Freeze-dried samples were analyzed using a PerkinElmer Spotlight 400 FT-IR Imaging System (Massachusetts, US). An attenuated total reflectance (ATR) accessory with diamond/ZnSe crystal was used for collecting 1024 scans with 4 cm^{-1} resolution in the case of chitosan-cellulose spheres, as the surface-level analysis was desired. A transmission base plate and KBr pellets were used for collecting 128 scans with a resolution of 4 cm^{-1} in the case of the chitosan and propargylated chitosan powders. Data were processed with Spectrum 6 Spectroscopy Software (PerkinElmer, Massachusetts, US).

Raman spectroscopy

Raman spectra were acquired in the range of 4000–400 cm^{-1} using a Thermo Nicolet 6700 FT-IR spectrometer (Thermo Fisher, Massachusetts, US) with FT-Raman module, equipped with 1064 nm laser exciting radiation and InGaAs detector. The laser power at the sample was set to 0.40 W, and 480 scans with a resolution of 8 cm^{-1} were collected for each reported sample.

X-ray photoelectron spectroscopy (XPS)

Surface characterization of neat and propargylated chitosan powders, as well as cellulose-chitosan spheres, was carried out using the AXIS Ultra DLD Photoelectron spectrometer (Kratos Analytical, Manchester, UK), under neutralization. Samples were mounted on the sample holder with UHV compatible carbon tape, together with an in-situ reference of pure cellulose (Johansson et al. 2020) and pre-evacuated overnight. Surface elemental content was calculated from low-resolution wide scans, while C 1*s*, O 1*s*, and N 1*s* high-resolution regional spectra were utilized for more detailed chemical information. Data was collected from 2 to 4 locations for each sample. The data was analyzed using CasaXPS software, with the C–O component of high-resolution C 1*s* signal at 286.7 eV as the binding energy reference (Beamson and Briggs 1992; Johansson and Campbell 2004).

Elemental analysis (EA)

Freeze-dried samples were processed in an ECS 4010 Elemental Combustion System CHNS-O from Costech Analytical technologies, Inc (Firenze, Italy) and data analyzed with the ECS60 software. Nitrogen- and Carbon content were collected and fitted into standard

curves with correlations of 0.99996 and 0.99998 for N and C, respectively. C/N molar ratio is reported.

Thermogravimetric analysis (TGA)

Freeze-dried samples were tested on aluminum pans in a TGA-50 Shimadzu Thermogravimetric Analyzer (Kyoto, Japan). Samples were heated from room temperature to 600 °C at a rate of 10 °C/min under compressed air flow at a rate of 20 mL/min. The thermograms and their corresponding first derivatives were recorded for each sample using the software TA-60WS.

Scanning electron microscopy (SEM)

Freeze-dried chitosan-cellulose and propargylated chitosan-cellulose spheres were smeared on aluminum studs and sputtered with gold in an EMS 550X Sputter Coating Device from Science Services (Munich, Germany). Images with a magnification of 50X, 100X, and 1000X were recorded in a Zeiss Evo 50VP scanning electron microscope (Oberkochen, Germany).

Fluorescence microscopy

The beads subjected to click chemistry reaction were analyzed using fluorescence and bright-filed microscopy. For that purpose, air-dried samples were placed on a coverslip and imaged at 10 × magnification, using an Olympus BX53 fluorescence microscope (Kyoto, Japan) equipped with an X-cite Series 120Q (Lumen dynamics) fluorescence illumination system and an Olympus DP73 camera. The images were obtained using BF- and FTIC filter cubes in the light path, respectively. The bright-field images were obtained by illuminating the samples with an external led source.

Fluorescence spectroscopy

The set of samples analyzed with the Olympus BX53 was also analyzed using a PerkinElmer® LS55 Luminescence Spectrometer (Beaconsfield, UK). The fluorescence emission spectra were recorded in the range of wavelengths between 510 and 610 nm, using an excitation wavelength set at 488 nm.

Results and discussion

Characteristics of the propargylated chitosan

After the chemical reaction, the resulting powder acquired an orange/red shade (Figure S1), which could be related to the presence of the propargyl groups linked to the amino groups in the C-2 of the chitosan backbone. Additionally, the studies on the solubility of the samples in water and 1% acetic acid showed differences between chitosan and its derivative, indicating that a chemical reaction took place. It was observed that the propargylated chitosan powder took longer to dissolve, and after 4% w/w, it was neither soluble in water nor 1% acetic acid, while unmodified chitosan was easily dissolved in 1% acetic acid, as expected.

Chemical composition

When the FTIR- and Raman spectra are evaluated (Fig. 2a), the most evident difference between unmodified chitosan and propargylated chitosan is the Raman band around 2100 cm^{-1} attributed to carbon–carbon triple bond (C≡C) stretching vibration, in the spectrum of the propargylated chitosan. Additionally, the intensity of the FTIR bands characteristic for the primary amine groups around 1600 cm^{-1} was significantly reduced for the propargylated chitosan.

XPS spectra of unmodified chitosan and the propargylated chitosan derivative, together with the cellulose (as reference), are shown in Fig. 2b. Apart from the expected carbon, oxygen, and nitrogen, only traces of Br and Mg in the propargylated sample (remnants from the derivatization process) are observed. An increase in the C–C component of the C1*s* signal of chitosan while compared to the cellulose reference is expected, due to carbonaceous passivation layers induced on carbohydrate surfaces in ultra-high vacuum and water-free environment (Johansson et al. 2011). There is a slight increase in the C–C component and a slight decrease in nitrogen content, both in the propargylated sample. The high-resolution peaks presented in the insert show this increase more clearly as the percentage increased from 19.8 to 36.1% (Table S1) after the modification. Otherwise, elemental surface compositions remain similar. Comparable results are observable in Table 1, which summarizes the results obtained from elemental analysis. Here, the propargylated chitosan presented a lower

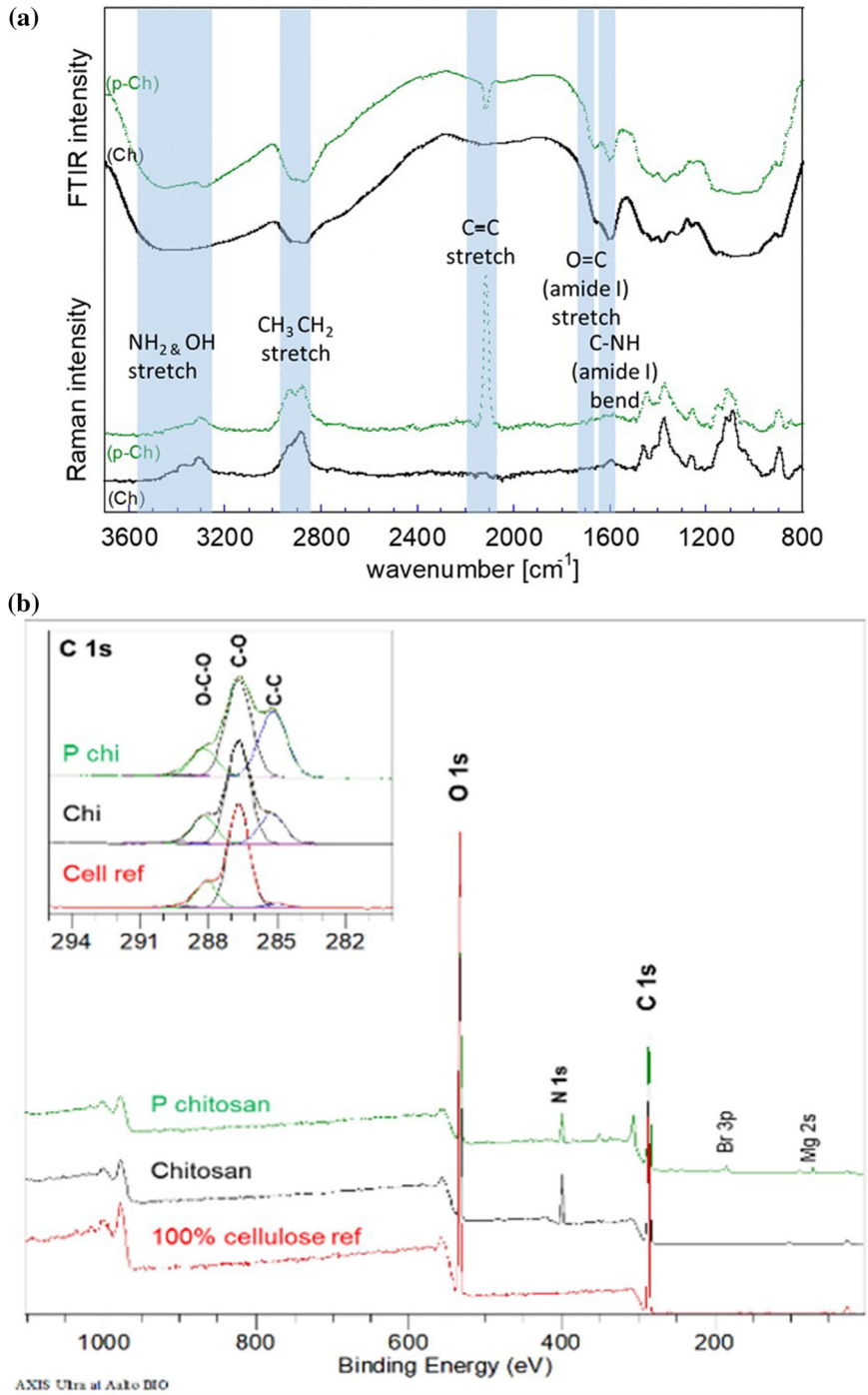

Fig. 2 Chemical characterization of chitosan (Ch) and propargylated chitosan (p-Ch). **a** FT-IR transmission spectra and Raman spectra and **b** XPS wide spectra of Ch and p-Ch powders, together with a cellulose reference (100% cellulose Whatman filter paper). The high-resolution carbon C1s region in the insert shows C–O and O–C–C components in a ratio characteristic of both cellulose and chitosan

Table 1 Elemental analysis of the unmodified chitosan and chitosan derivative, and the formed spherical beads

Sample	N (%)	C (%)	C:N
Dissolving pulp	n/a	42.1	n/a
Chitosan	7.3	41.0	6.5
Propargylated chitosan	6.4	52.8	9.7
Chitosan-cellulose spheres	1.4	40.1	35.6
Propargylated chitosan-cellulose spheres	2.3	44.9	22.6

nitrogen content with a simultaneous increase of the C:N ratio, which can be explained based on the propargyl group bonded to the NH_2 residue in C-2 of chitosan, as confirmed by FTIR analysis and seen in the XPS change of ratios.

The degree of substitution (DS) was determined by following the increase in carbon content of propargylated chitosan (elemental analysis). The carbon content of unmodified chitosan increased from 41 to 52.8% due to the installation of propargyl moieties. This increase (11.8%) was used to calculate the grafting density of propargylated chitosan sample. It was found that 75% of available amino groups reacted with propargyl bromide which in turn corresponds to a DS value of 0.64. It is worth mentioning that the maximum DS for a given sample is 0.85 as it possesses 15% of acetylated amino groups.

Thermogravimetric properties

Additional evidence of successful chitosan chemical modification was obtained by analyzing the thermal stability of the chitosan and its propargylated derivative. Figure 3 shows the thermograms of the corresponding samples. It can be observed that the propargylated chitosan derivative presents a lower onset degradation temperature (234 °C) when compared to that of unmodified chitosan (264 °C), respectively. The maximum degradation temperature observed at 345 °C corresponds to the unmodified chitosan. It is also worth mentioning that in the case of propargylated chitosan, a drastic weight loss was recorded at 268 °C. This difference in behavior is observed in multiple chitosan derivatives, as the rate of degradation of the native amino groups is slower than the added moieties (Chivangkul et al. 2014; Tan et al. 2018); furthermore, the rapid thermal degradation observed of the installed propyne groups behaves similar to other small groups on chitosan (Chen et al. 2015b).

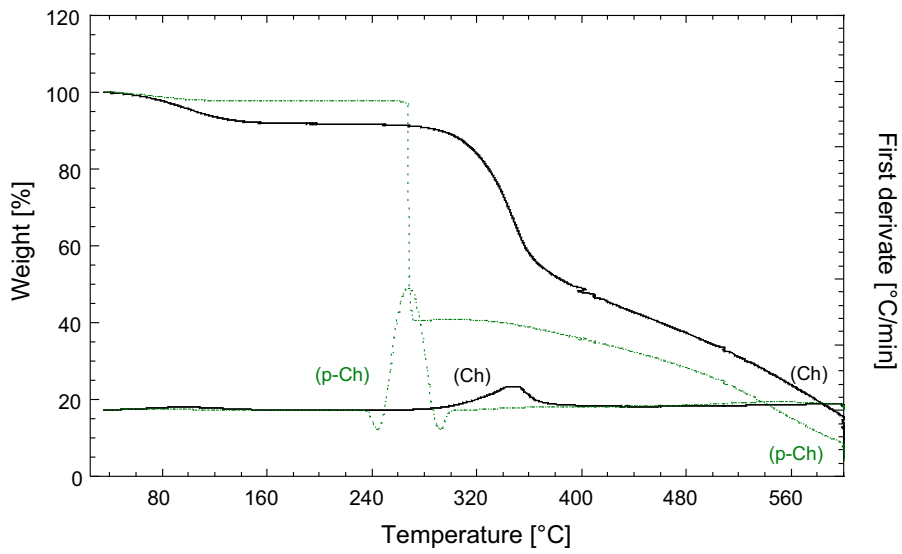

Fig. 3 Results from the thermogravimetric analysis of the powders from chitosan (Ch) and propargylated chitosan (p-Ch)

Characterization of the functionalized spherical beads

To produce 3-D structures that could be useful in target applications such as immobilization of macromolecules, spherical beads were formed. For that purpose, Ch or p-Ch powders were added to the sodium-urea solution containing dissolved cellulose, at − 10 °C. This mixture aimed to have a homogeneous blend of the polymers on the surface. Figure 4 shows the chitosan cellulose spheres obtained with this approach. As the cellulose solution drop falls into the acid bath for cellulose coagulation, the drops decrease in diameter as they travel through the regeneration media, forming a more homogeneous structure until the final spherical shape is obtained.

The newly formed spheres had an average weight of 29.4 ± 4.02 mg, and after thoroughly drying, the weight dropped to 1.03 ± 0.49 mg, showing an excellent water retention capability of almost 300% w/w. As shown in Fig. 4, the diameter of the spheres was 2.66 ± 0.09 mm, which results in a density of 0.10 g/cm^3.

Water retention and water uptake capacity measurements

Water interactions were evaluated after completely drying. The chitosan-cellulose spheres were submerged in ultrapure water, in a 15 mM NaCl solution, and in standard PBS buffer (ca. 150 mM) to measure the re-swelling capabilities. These spheres only doubled their weight when measured in water and 15 mM NaCl, increasing to 2 mg. However, for the PBS buffer, the weight of the spheres went up to approximately 4 mg, having a different behavior in the highly saline environment. This capacity to re-swell, even if limited, can be explained by the initial high porosity of the sample and the presence of the chitosan; both might prevent the fibers from completely collapsing during the drying process, allowing some water uptake.

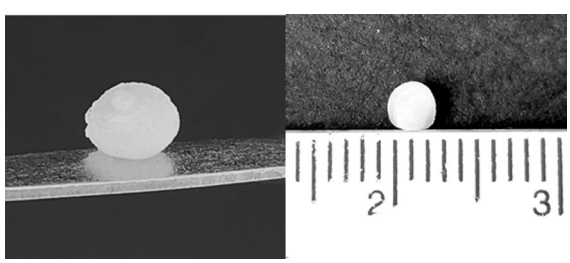

Fig. 4 Spheres obtained after the regeneration of the cellulose-chitosan blend

Chemical composition

FTIR spectra for the chitosan cellulose spheres and the propargylated chitosan-cellulose spheres show almost no differences (Fig. 5a). The most notable difference is the decrease of the bands at 1640 and 1590 cm^{-1} observed in the spectrum of propargylated spheres, both attributed to a decrease in the N–H deformation in amino group vibrations (Figure S2). The results can be taken as an indication of the successful modification of the C-2 amino groups of chitosan. Moreover, data obtained from the elemental analysis (Table 1) revealed an increase in nitrogen content of the propargylated chitosan-cellulose spheres (2.3%) when compared to that of the chitosan-cellulose spheres (1.4%). The nitrogen content of spheres is lower than that of the propargylated chitosan and it can be explained by the presence of cellulose component in the spheres. Meanwhile, XPS wide energy region spectra (Fig. 5b) showed the evident decrease of the N signal, further confirming the different composition of the beads. In contrast, the high-resolution C 1*s* spectra showed an increase on the C–C curve of 16.2% (Table S1), when compared with the cellulose reference, indicating that the alkyl group of the propargyl is present in the surface.

Thermogravimetric analysis

From the thermal analysis of both spheres (Fig. 6), the chitosan-cellulose spheres show an onset temperature of 312 °C. In contrast, the propargylated chitosan cellulose spheres presented a much lower onset temperature of 251 °C, related to the presence of the efficiently degraded propargyl chitosan powder, as discussed earlier. From the first derivative of the thermograms, it can be observed that the chitosan-cellulose spheres presented a clear maximum peak around 264 °C, related to the degradation of pure chitosan, and a second peak at 382 °C, close to the maximum degradation temperature of pure dissolving pulp. The presence of two peaks further confirms that we have two independent components in the structure. However, the propargylated chitosan-cellulose

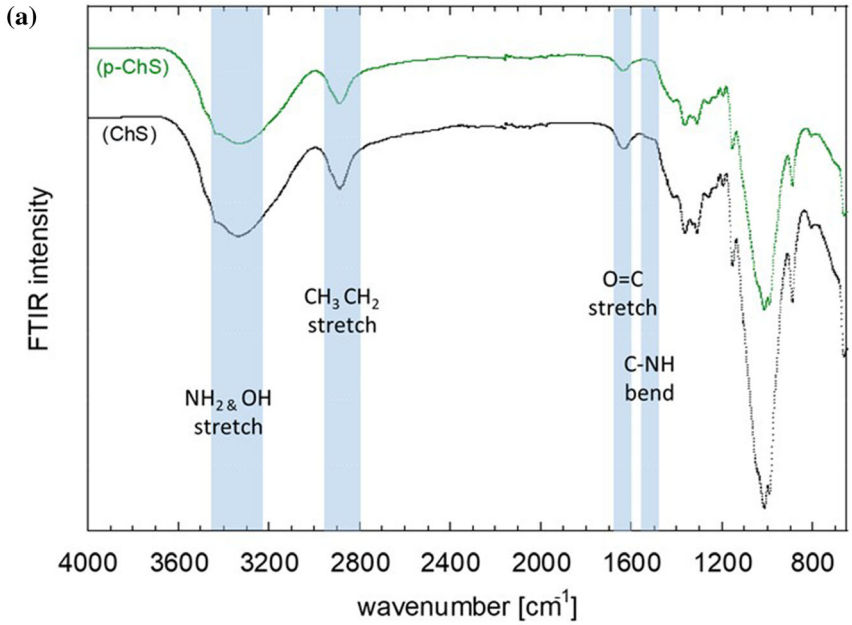
(a)
(p-ChS)
(ChS)
FTIR intensity
NH2 & OH stretch
CH3 CH2 stretch
O=C stretch
C-NH bend
4000 3600 3200 2800 2400 2000 1600 1200 800
wavenumber [cm-1]

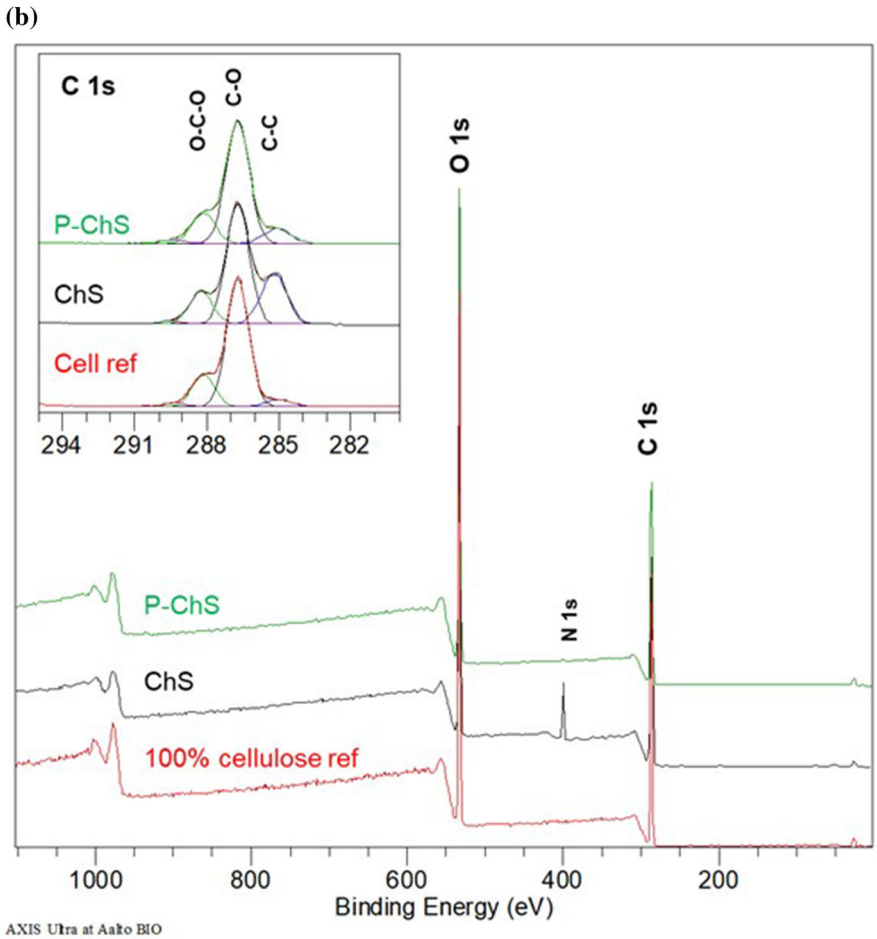
(b)
C 1s
O-C-O
C-O
C-C
P-ChS
ChS
Cell ref
294 291 288 285 282
O 1s
C 1s
N 1s
P-ChS
ChS
100% cellulose ref
1000 800 600 400 200
Binding Energy (eV)
AXIS Ultra at Aalto BIO

◀**Fig. 5** Chemical characterization of chitosan-cellulose spheres (ChS) and propargylated chitosan-cellulose spheres (p-ChS). **a** FT-IR transmission spectra and **b** XPS wide spectra of chitosan-cellulose spheres (ChS) and propargylated chitosan-cellulose spheres (ChS), together with a cellulose reference (100% cellulose Whatman filter paper). The high-resolution carbon C 1*s* region in the insert shows C–O and O–C–C components in a ratio characteristic of both cellulose and chitosan

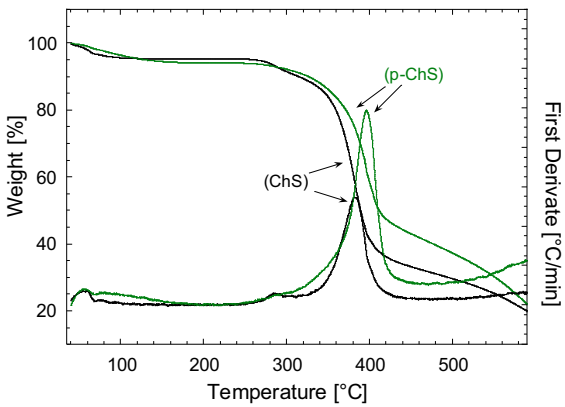

Fig. 6 Comparison of TGA of chitosan-cellulose spheres (ChS) and propargylated chitosan-cellulose spheres (p-ChS)

spheres showed only one high-intensity peak at 396 °C, indicating a better cohesion between the two polymers, and the possible interaction between them. This could be related to the hydrophobic nature of the triple bond (Chen et al. 2015a). This is particularly true for the derivatized chitosan, which would require more energy to be in solution; therefore, these two polymers, with different surface energies would try to decrease their energy by adsorbing onto each other, facilitating miscibility and thus facilitating the interactions of the propargylated chitosan with the surface of the dissolving pulp (Teramoto 2015).

When analyzing the morphology of the spheres (Fig. 7) by SEM, a smoother surface is observed in the case of propargylated chitosan cellulose spheres. This characteristic could relate to an improved interaction between the polymers during the synthesis of the spheres, supporting the observations found in the thermal analysis.

These performed tests showed that the methodology used to generate the sphere-like beads has no adverse effect on the presence of the active groups on the surface.

Viability of the alkyne functional groups on the propargylated-chitosan spheres

Even with the presence of the new functional groups, its viability on surface for modification is imperative for future applications. To assess this, fluorescence tagging was performed. The results from the fluorescence emission spectra and fluorescence microscopy images have provided experimental evidence to support our hypothesis that the alkyl functional groups on p-ChS beads can react with azide moieties in aqueous media. As can be observed in Fig. 8, the presence of fluorescent moieties is evident in the p-ChS* beads, which were prepared by treating p-ChS with A488 in the presence of Cu(I). Moreover, comparing these two spectra (Fig. 9), it is possible to notice a clear difference in their maximum emission wavelengths, which might occur due to the changes at the molecular level after the alkyne-azide coupling reaction. By contrast, the emission spectrum of the ChS* does not show the characteristic peak at 524 nm, demonstrating that dye was not covalently linked to the ChS beads, and that can be easily removed from these by washing. Finally, the emission spectrum of p-ChS (beads never exposed to A488) shows that this material is not responsible for the peak observed in the case of p-ChS*. These results agree with the hypothesis that the alkyl functional groups on the surface of the p-ChS beads can be coupled with the azide functional groups of A488 via click chemistry reaction.

As the added functional groups are still viable in the system described, the possible uses of these beads can range widely. These beads can be useful in many of the aforementioned applications such as catalytic reactors (Luo and Zhang 2010; Filpponen et al. 2012; Vega Erramuspe et al. 2016), bio-based single-use sensors (Qiu et al. 2013), sophisticated colorimetric devices using other proteins as a secondary market such as green fluorescent protein (Wei et al. 2010; Bhopate et al. 2015) or immobilizing quantum dots that provide synergy with target enzymes to improve sensing (Junka et al. 2014; Iñarritu et al. 2017). All of these with less steps that other alternatives presented before, lowering cost and carbon footprint.

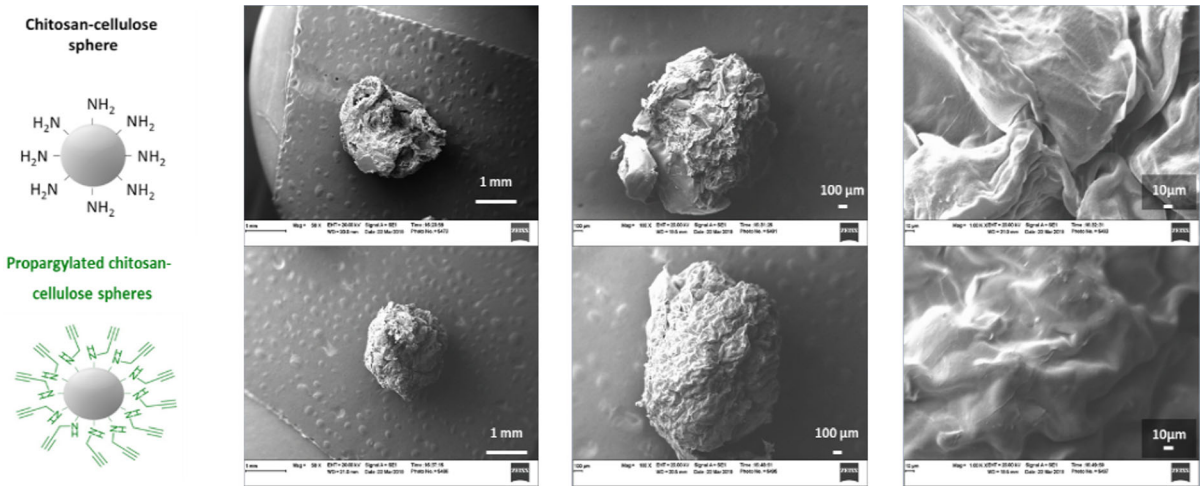

Fig. 7 Scanning electron microscopy images of the chitosan-cellulose spheres and the propargylated chitosan-cellulose spheres

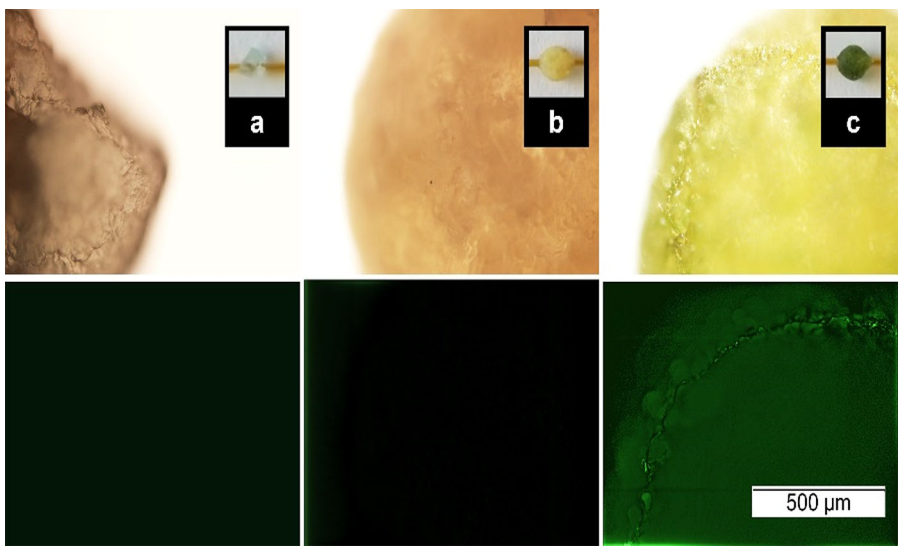

Fig. 8 Pictures of ChS* (**a**), p-ChS (**b**), and p-ChS* (**c**). The samples marked with an asterisk were treated with Azide-fluor488 fluorescent dye, in the presence of Cu(I) and under the same experimental conditions. The bright-field images with 10 × magnification (top row) and the fluorescent images with 10 × magnification (bottom row) were collected with an Olympus BX53 fluorescent microscope. An FTIC filter cube was used to observe the fluorescence. ChS, cellulose beads, p-ChS; propargylated chitosan-cellulose beads

Conclusions

This work demonstrates that the addition of propyne groups into cellulose-based beads with the simple approach of mixing pre-modified chitosan before regeneration to make the beads susceptible to click chemistry. This relatively easy methodology allows to retain the active groups on the surface. throughout the formation process and therefore these can be used as anchoring points for reactive molecules bearing propyne functional groups, as it was shown with the commercial dye A488.

The generation of sphere-shaped cellulose beads in the presence of a chitosan derivative showed a simple and reproducible method for the functionalization of the cellulose beads. The easy blending of the chitosan derived can be used as a tool for tunning the density and availability of the clickable moieties by differing

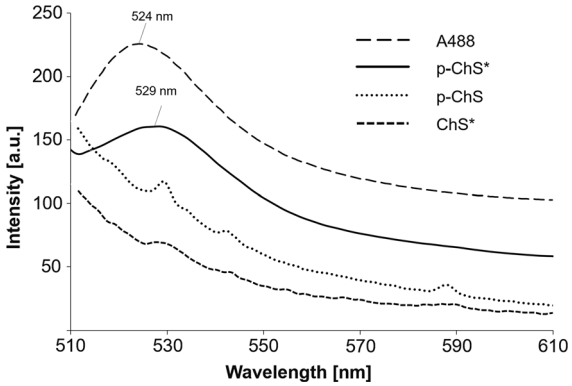

Fig. 9 Fluorescence spectra of Alexa-fluor 488 commercial dye (A488) in a diluted solution and the solid samples p-ChS*, pChS, and ChS*. The samples marked with an asterisk were treated with A488 in the presence of Cu(I) in aqueous solutions and under the same experimental conditions. p-ChS, propargylated chitosan-cellulose beads; ChS, chitosan-cellulose beads

concentrations of the modified polysaccharide are added to the blend Thus, these beads can be used search for a wide-ranging generation of green products as scaffolds for high-end applications via click chemistry with little modification to the structure that aim to be immobilized, such as the clicking of proteins or other active components. This can then be achieved with short steps improving production costs and times.

Acknowledgments This work was supported by the USDA National Institute of Food and Agriculture, Hatch program (ALA013-17003) and McIntire-Stennis program (1022526). The School of Forestry and Wildlife Sciences at Auburn University's financial support to complete this work is much appreciated. This work made use of Aalto University Bioeconomy Facilities (the XPS statement).

Authors contribution The manuscript was written through the contributions of all authors. All authors have approved the final version of the manuscript. Apart from the XPS measurements and analysis (conducted by Johansson), and click chemistry and fluorescence measurements, with the corresponding analysis (conducted by Vega), all the authors have contributed equally.

Declarations

Conflict of Interest The authors declare no conflict of interest.

References

Bart J, Tiggelaar R, Yang M et al (2009) Room-temperature intermediate layer bonding for microfluidic devices. Lab Chip 9:3481–3488. https://doi.org/10.1039/b914270c

Beamson G, Briggs D (1992) High resolution XPS of organic polymers: the Scienta ESCA 300 database. Wiley, Chichester

Bhopate DP, Mahajan PG, Garadkar KM et al (2015) A highly selective and sensitive single click novel fluorescent off–on sensor for copper and sulfide ions detection directly in aqueous solution using curcumin nanoparticles. New J Chem 39:7086–7096. https://doi.org/10.1039/C5NJ01228G

Binder W, Kluger C (2006) Azide/Alkyne-"Click" reactions: applications in material science and organic synthesis. Curr Org Chem 10:1791–1815. https://doi.org/10.2174/138527206778249838

Blachechen LS, Fardim P, Petri DFS (2014) Multifunctional cellulose beads and their interaction with gram positive bacteria. Biomacromol 15:3440–3448. https://doi.org/10.1021/bm5009876

Burnaevskiy N, Fox TG, Plymire DA et al (2013) Proteolytic elimination of N-myristoyl modifications by the Shigella virulence factor IpaJ. Nature 496:106–109. https://doi.org/10.1038/nature12004

Cai J, Zhang L (2006) Unique gelation behavior of cellulose in NaOH/urea aqueous solution. Biomacromol 7:183–189. https://doi.org/10.1021/bm0505585

Chen J, Lin N, Huang J, Dufresne A (2015a) Highly alkynyl-functionalization of cellulose nanocrystals and advanced nanocomposites thereof via click chemistry. Polym Chem 6:4385–4395. https://doi.org/10.1039/c5py00367a

Chen Y, Ye Y, Jing Y et al (2015b) The synthesis of the locating substitution derivatives of chitosan by click reaction at the 6-position of chitin. Int J Polym Sci. https://doi.org/10.1155/2015/419506

Chivangkul T, Pengprecha S, Padungros P et al (2014) Enhanced water-solubility and mucoadhesion of N, N, N-trimethyl-N-gluconate-N-homocysteine thiolactone chitosan. Carbohydr Polym 108:224–231. https://doi.org/10.1016/j.carbpol.2014.02.078

de Carvalho RA, Veronese G, Carvalho AJF et al (2016) The potential of TEMPO-oxidized nanofibrillar cellulose beads for cell delivery applications. Cellulose 23:3399–3405. https://doi.org/10.1007/s10570-016-1063-2

Elsayed S, Hellsten S, Guizani C et al (2020) Recycling of superbase-based ionic liquid solvents for the production of textile-grade regenerated cellulose fibers in the lyocell process. ACS Sustain Chem Eng 8:14217–14227. https://doi.org/10.1021/acssuschemeng.0c05330

Filpponen I, Kontturi E, Nummelin S et al (2012) Generic method for modular surface modification of cellulosic materials in aqueous medium by sequential "click" reaction and adsorption. Biomacromol 13:736–742. https://doi.org/10.1021/bm201661k

French AD (2017) Glucose, not cellobiose, is the repeating unit of cellulose and why that is important. Cellulose 24:4605–4609. https://doi.org/10.1007/s10570-017-1450-3

Fujii Y, Imagawa K, Omura T et al (2020) Preparation of cellulose/silver composite particles having a recyclable catalytic property. ACS Omega 5:1919–1926. https://doi.org/10.1021/acsomega.9b03634

Gericke M, Trygg J, Fardim P (2013) Functional cellulose beads: preparation, characterization, and applications. Chem Rev 113:4812–4836. https://doi.org/10.1021/cr300242j

Gonçalves C, Pereira P, Gama M (2010) Self-assembled hydrogel nanoparticles for drug delivery applications. Materials (basel) 3:1420–1460. https://doi.org/10.3390/ma3021420

Guan L, van der Heijden GW, Bortvin A, Greenberg MM (2011) Intracellular detection of cytosine incorporation in genomic DNA by using 5-ethynyl-2′-deoxycytidine. ChemBioChem 12:2184–2190. https://doi.org/10.1002/cbic.201100353

Guo J, Filpponen I, Su P et al (2016) Attachment of gold nanoparticles on cellulose nanofibrils via click reactions and electrostatic interactions. Cellulose 23:3065–3075. https://doi.org/10.1007/s10570-016-1042-7

Hoyle CE, Bowman CN (2010) Thiol-ene click chemistry. Angew Chem Int Ed 49:1540–1573. https://doi.org/10.1002/anie.200903924

Hu L, Zhao P, Deng H et al (2014) Electrical signal guided click coating of chitosan hydrogel on conductive surface. RSC Adv 4:13477–13480. https://doi.org/10.1039/c3ra47507g

Ifuku S, Wada M, Morimoto M, Saimoto H (2011) Preparation of highly regioselective chitosan derivatives via "click chemistry." Carbohydr Polym 85:653–657. https://doi.org/10.1016/j.carbpol.2011.03.030

Ifuku S, Matsumoto C, Wada M et al (2013) Preparation of highly regioselective amphiprotic chitosan derivative via "Click chemistry." Int J Biol Macromol 52:72–76. https://doi.org/10.1016/j.ijbiomac.2012.08.012

Iñarritu I, Torres E, Topete A, Campos-Terán J (2017) Immobilization effects on the photocatalytic activity of CdS quantum Dots-Horseradish peroxidase hybrid nanomaterials. J Colloid Interface Sci 506:36–45. https://doi.org/10.1016/j.jcis.2017.07.015

Johansson LS, Campbell JM (2004) Reproducible XPS on biopolymers: cellulose studies. Surf Interface Anal 36:1018–1022. https://doi.org/10.1002/sia.1827

Johansson LS, Tammelin T, Campbell JM et al (2011) Experimental evidence on medium driven cellulose surface adaptation demonstrated using nanofibrillated cellulose. Soft Matter 7:10917–10924. https://doi.org/10.1039/c1sm06073b

Johansson LS, Campbell JM, Rojas OJ (2020) Cellulose as the in situ reference for organic XPS. Why? Because it works. Surf Interface Anal 52:1–5. https://doi.org/10.1002/sia.6759

Junka K, Guo J, Filpponen I et al (2014) Modification of cellulose nanofibrils with luminescent carbon dots. Biomacromol 15:876–881. https://doi.org/10.1021/bm4017176

Kolb HC, Finn MG, Sharpless KB (2001) Click chemistry: diverse chemical function from a few good reactions. Angew Chem Int Ed Engl 40:2004–2021

Kulbokaite R, Ciuta G, Netopilik M, Makuska R (2009) N-PEG'ylation of chitosan via "click chemistry" reactions. React Funct Polym 69:771–778. https://doi.org/10.1016/j.reactfunctpolym.2009.06.010

Kumar Dutta P, Dutta J, Tripathi VS (2004) Chitin and chitosan: chemistry, properties and applications. J Sci Ind Res 63:20–31. https://doi.org/10.1002/chin.200727270

Laughlin ST, Baskin JM, Amacher SL, Bertozzi CR (2008) In vivo imaging of membrane-associated glycans in developing zebrafish. Science 320:664–667. https://doi.org/10.1126/science.1155106

Liang L, Astruc D (2011) The copper(I)-catalyzed alkyne-azide cycloaddition (CuAAC) "click" reaction and its applications. An Overview Coord Chem Rev 255:2933–2945. https://doi.org/10.1016/j.ccr.2011.06.028

Luo X, Zhang L (2010) Creation of regenerated cellulose microspheres with diameter ranging from micron to millimeter for chromatography applications. J Chromatogr A 1217:5922–5929. https://doi.org/10.1016/j.chroma.2010.07.026

Luo X, Lei X, Cai N et al (2016) Removal of heavy metal ions from water by magnetic cellulose-based beads with embedded chemically modified magnetite nanoparticles and activated carbon. ACS Sustain Chem Eng 4:3960–3969. https://doi.org/10.1021/acssuschemeng.6b00790

O'Neill Jr JJ, Reichardt EP (1951) Method of producing cellulose pellets. US Patent 2543928A

Orelma H, Filpponen I, Johansson LS et al (2011) Modification of cellulose films by adsorption of CMC and chitosan for controlled attachment of biomolecules. Biomacromol 12:4311–4318. https://doi.org/10.1021/bm201236a

Park S, Kim SH, Kim JH et al (2015) Application of cellulose/lignin hydrogel beads as novel supports for immobilizing lipase. J Mol Catal B Enzym 119:33–39. https://doi.org/10.1016/j.molcatb.2015.05.014

Pinkert A, Marsh KN, Pang S (2010) Reflections on the solubility of cellulose. Ind Eng Chem Res 49:11121–11130. https://doi.org/10.1021/ie1006596

Qiu S, Li X, Xiong W et al (2013) A novel fluorescent sensor for mutational p53 DNA sequence detection based on click chemistry. Biosens Bioelectron 41:403–408. https://doi.org/10.1016/j.bios.2012.08.065

Reis DT, Pereira AKDS, Scheidt GN, Pereira DH (2019) Plant and bacterial cellulose: production, chemical structure, derivatives and applications. Orbital 11:321–329. https://doi.org/10.17807/orbital.v11i5.1349

Reyes G, Lundahl MJ, Alejandro-Martín S et al (2020) Coaxial spinning of all-cellulose systems for enhanced toughness: filaments of oxidized nanofibrils sheathed in cellulose II regenerated from a protic ionic liquid. Biomacromol 21:878–891. https://doi.org/10.1021/acs.biomac.9b01559

Rinaudo M (2006) Chitin and chitosan: properties and applications. Prog Polym Sci 31:603–632. https://doi.org/10.1016/j.progpolymsci.2006.06.001

Rojas OJ (2014) Outlook for Nanocellulose Production and Materials. Funct Nanomater Anticaking Agent Antimicrob Filtr Hardness Sorbent 2017:1–22

Singh S, Shauloff N, Jelinek R (2019) Solar-enabled water remediation via recyclable carbon dot/hydrogel composites. ACS Sustain Chem Eng 7:13186–13194. https://doi.org/10.1021/acssuschemeng.9b02342

Struszczyk MH (2002) Chitin and chitosan. Polimery 47:316–325. https://doi.org/10.1002/0471440264.pst052

Tan W, Li Q, Dong F et al (2018) Novel cationic chitosan derivative bearing 1,2,3-triazolium and pyridinium: synthesis, characterization, and antifungal property. Carbohydr Polym 182:180–187. https://doi.org/10.1016/j.carbpol.2017.11.023

Tan Y, Wu H, Xie T et al (2020) Characterization and antibacterial effect of quaternized chitosan anchored cellulose beads. Int J Biol Macromol 155:1325–1332. https://doi.org/10.1016/j.ijbiomac.2019.11.104

Teramoto Y (2015) Functional thermoplastic materials from derivatives of cellulose and related structural polysaccharides. Molecules 20:5487–5527. https://doi.org/10.3390/molecules20045487

Trivedi P, Saloranta-Simell T, Maver U et al (2018) Chitosan-Cellulose multifunctional hydrogel beads: design, characterization and evaluation of cytocompatibility with breast adenocarcinoma and osteoblast cells. Bioengineering 5:3. https://doi.org/10.3390/bioengineering5010003

Trygg J, Fardim P, Gericke M et al (2013) Physicochemical design of the morphology and ultrastructure of cellulose beads. Carbohydr Polym 93:291–299. https://doi.org/10.1016/j.carbpol.2012.03.085

Trygg J, Yildir E, Kolakovic R et al (2014) Anionic cellulose beads for drug encapsulation and release. Cellulose. https://doi.org/10.1007/s10570-014-0253-z

Vega Erramuspe IB, Fazeli E, Näreoja T et al (2016) Advanced cellulose fibers for efficient immobilization of enzymes. Biomacromol 17:3188–3197. https://doi.org/10.1021/acs.biomac.6b00865

Voon LK, Pang SC, Chin SF (2015) Highly porous cellulose beads of controllable sizes derived from regenerated cellulose of printed paper wastes. Mater Lett 164:264–266. https://doi.org/10.1016/j.matlet.2015.10.161

Wei X, Qi L, Tan J et al (2010) Analytica Chimica Acta A colorimetric sensor for determination of cysteine by carboxymethyl cellulose-functionalized gold nanoparticles. Anal Chim Acta 671:80–84. https://doi.org/10.1016/j.aca.2010.05.006

Wittmar ASM, Böhler H, Kayali AL, Ulbricht M (2020) One-step preparation of porous cellulose/chitosan macrospheres from ionic liquid-based solutions. Cellulose 27:5689–5705. https://doi.org/10.1007/s10570-020-03165-y

Wu J, Andrews MP (2020) Carboxylated cellulose nanocrystal microbeads for removal of organic dyes from wastewater: effects of kinetics and diffusion on binding and release. ACS Appl Nano Mater. https://doi.org/10.1021/acsanm.0c02353

Zambrano F, Wang Y, Zwilling JD et al (2020) Micro- and nanofibrillated cellulose from virgin and recycled fibers: a comparative study of its effects on the properties of hygiene tissue paper. Carbohydr Polym 254:117430. https://doi.org/10.1016/j.carbpol.2020.117430